Technical Report No. 3

THE ELECTRICAL RESISTIVITY OF COLD-WORKED ALUMINUM SINGLE CRYSTALS

Author: A. Sosin

Project Supervisor: J. S. Koehler

Board of Trustees
University of Illinois
Urbana, Illinois

Period Covered
Feb. 1, 1953 to May 1, 1954

Contract DA-11-022-ORD-1212
Project No. TB2-0001(756)

CHAPTER I

INTRODUCTION

A large amount of work has been devoted in recent years to the study of imperfections in solids. Whereas a number of physical properties have been investigated for this purpose, the electrical resistivity has probably been more widely exploited than any other. In a recent review article, Broom[1] has compiled the extensive work on electrical resistivity as well as describing other closely related work such as stored energy and stress-strain measurements. This paper will not attempt to restate this data; the reader is referred directly to Broom's article. Only data immediately related to this experiment will be discussed.

CHAPTER II

PRELIMINARY DISCUSSIONS

The list of imperfections possible in a lattice is considerable. Seitz[2] has labelled phonons, electrons and holes, excitons, vacant lattice sites (vacancies) and interstitial atoms (interstitials), foreign atoms, and dislocations as primary imperfections with light quanta, charged radiation and uncharged particles as transient imperfections. Calculations have been made of the effect of a particular imperfection on electrical resistivity.

Dislocations. The first calculation of the increase of resistivity due to dislocations was performed by Koehler[3]. The calculation has been subsequently corrected by Mackenzie and Sondheimer[4], Landauer[5] Hirone and Adachi[6], Dexter[7], Saenz[8], and Hunter and Nabarro[9]. According to the later calculations, dislocations should scatter conduction electrons anisotropically: there should be no additional scattering in the direction of the dislocation axis for either edge type or screw type dislocations whereas there will be scattering normal to this direction. For screw dislocations, scattering normal to the dislocation axis should be isotropic; for edge dislocations, the additional resistivity increase in the slip direction should be one-third that normal to the slip plane.

Dexter[7] has also calculated the magnitude of the resisitivity changes to be expected from edge dislocations. He requires on the order of 5×10^{12} pairs of positive and negative dislocations per square centimeter to account for the observed resistivity increase in heavily cold-worked copper. This is not in good agreement with

the estimate of Koehler[10] obtained from stored energy measurements. Hunter and Nabarro[9], referring to isotropic resistivity increases, calculate the following changes for copper (N is the number of dislocation lines/ cm.^{2})

Edge dislocations: $\Delta\rho = 0.59 \times 10^{-14} N\ \mu\Omega\text{-cm}$

Screw dislocations: $\Delta\rho = 0.18 \times 10^{-14} N\ \mu\Omega\text{-cm}$

"Average": $\Delta\rho = 0.39 \times 10^{-14} N\ \mu\Omega\text{-cm}$

These values also require about 5×10^{12} dislocation lines/cm.^{2}

Klemens[11] has also estimated the scattering of electrons due to stacking faults. He finds the scattering to be comparable to that of pure dislocations.

Vacancies. Dexter[12] has calculated the increase of resistance due to one atomic percent of vacancies in copper to be about 0.4 $\mu\Omega$-cm. Jongenburger[13] has criticised this calculation and obtained a value of 1.3 $\mu\Omega$-cm. It would also be interesting to have values for conglomerates. According to Seitz[14], conglomerates will scatter less than individual vacancies.

Interstitials. Dexter[12] has calculated the increase of resistance due to one atomic percent of interstitials in copper to be about 0.6 $\mu\Omega$-cm.

Studies of the recovery of resistivity have also been made. To interpret these data, reference can be made to the following calculations. Huntington and Seitz[15] and Huntington[16] have found the activation energy for movement of a single vacancy in copper to be about 1 ev. Seitz[14] suggested that the activation energy for a pair of vacancies should be lower than this value; calculations of Bartlett and Dienes[17] confirm this, showing an activation energy for a pair to be somewhat less than 1 ev. They also calculated the

energy required to dissociate a pair to be between 0.25 and 0.59 ev. This implies some pairing should occur. The activation energy for motion of single interstitials was calculated by Huntington to be between 0.07 ev. and 0.24 ev. in copper. It is difficult to define an activation energy for dislocations.

We are here most concerned with the effect of deformation on the electrical resistivity. It is now generally accepted that work-hardening is due to the motion and generation of dislocations and the subsequent generation of vacancies and interstitials as well as the interaction of these defects. In fact, it is the ultimate purpose of this work to arrive at a reasonable picture of these events.

In deforming a metal to measure the resistivity, it is important to note that, unless the deformation is done at a sufficiently low temperature, simultaneous recovery will occur. This was first brought out clearly by the experiments of Molenaar and Aarts[18]. They pulled soft-annealed wires of copper, silver, and aluminum to about ten percent extension in a liquid nitrogen bath ($78^{\circ}K$), warmed to room temperature ($300^{\circ}K$) for periods ranging between ten minutes and eighteen hours, then pulled further in the bath. They observed the ordinary stress-strain behavior with no apparent effect due to the warming. However, the resistivity, which increased in the first loading, dropped upon warming, then rose with further strain. They concluded that the work hardening mechanism "is at least in part different from that producing the change in resistivity".

This work was extended by Druyvesteyn and Manintveld[19] and by Manintveld[20]. Wires of copper, silver and gold were strained at 78° K, then annealed to various temperatures for 15 and 45 minute

intervals. Two recovery processes are distinguishable in this manner. For copper, one recovery takes place in the range of -110° C with an activation energy of 0.20 ± 0.03 ev; the other takes place in the range of 0° C with an activation energy of 0.88 ± 0.09 ev. In a personal communication, Manintveld states that recovery takes place in aluminum at 78° K. The authors have suggested that the high temperature is due to the diffusion of single vacancies and the low temperature recovery is due to the conglomeration of vacancies. Under the assumption of single vacancy diffusion, they arrived at a diffusion "radius" of about 1 micron-- a figure usually associated with mosaic block lengths.

The above work was done on polycrystalline material. Blewitt, Redman, and Sherrill[21] have deformed single crystals of copper at 4° K, 78° K, and 300° K. They were unable to detect any resistance changes for strains less than .25. For larger strains at 78° K, the recoverable portion of the resistance after an hour anneal at 300° K depended upon the amount of strain. They also found no temperature dependence of the critical shear stress over the entire temperature region; the stress-strain curve is linear. In addition, they observed a strain--aging phenomenon in crystals extended at 78° K.

Eggleston[22] has twisted 10 mil copper wires in a liquid helium bath (4° K). He also finds two anneals between -140° C and 20° C with activation energies of 0.44 ± 0.06 ev and 0.67 ± 0.09 ev. These results should be compared with those of Overhauser[23] who irradiated copper with 12 Mev deuterons at 78° K. Overhauser found a high-temperature recovery near -60° C with an activation energy of 0.68 ± 0.02 ev. He also found a recovery which extended over a

wide temperature range to which he assigned an average activation energy of 0.44 ev at about -100° C. Furthermore, Overhauser was able to account for the higher temperature recovery by a second-order reaction suggesting the recombination of vacancies and interstitials. One-half of the resistivity increase recovered in the range of -185° C and -60° C; one quarter recovered between -60° C and room temperature. Annealing to 167° C produced only an additional four percent recovery.

It would also be desirable to correlate the resistivity increases with a quantity such as stress and strain. Weyerer[24] has found that the resistivity-extension curve saturates for loading at 300° K, indicating defect production and simultaneous annealing seem to balance. However, van Beuren[25] quotes unpublished results of Manintveld showing that $\Delta\rho \propto \epsilon^{3/2}$ where ϵ is the percent elongation; van Bueren is able to account for this theoretically. He proposes that $\Delta\rho = A\epsilon^{1/2} + B\epsilon^{3/2}$ where $A\epsilon^{1/2}$ is the dislocation resistance and $B\epsilon^{3/2}$ is the vacancy or interstitial resistance. Thus he claims that the electron scattering is due entirely to vacancies and interstitials.

Pry and Hennig[26], working on copper at -195° C and annealing at room temperature between strain increments, find that the recoverable resistivity at each period is linearly proportional to the unrecoverable portion. Blewitt also reports this result. This may say that the recoverable portion is produced by the unrecoverable portion and depends on the density of latter generators (i.e., vacancies and interstitials being produced by dislocations and annealing).

From these data, it is obvious that it would be of consider-

able interest to determine more directly the mechanism of resistivity increase. Realizing that the scattering of electrons by vacancies and interstitials, edge dislocations, screw dislocations, stacking faults, etc. should have different symmetry properties, it is suggested that one should look for the anisotropic behavior of the resistivity. This is, indeed, the primary concern of the present investigation.

Some investigation of this effect has been made. Broom[27] and Broom and Clothier[28] measured the resistivity of heavily cold-rolled strips of several metals and alloys. Using a calibrated current flow pattern, they attempted to statistically analyze the resistivity for anisotropic effects. Any observed effects were small and the longitudinal resistivity was greater than, equal to, or smaller than the transverse resistivity, depending on the material. Broom[1] also tells of work of Berghout on thin strips deformed lightly in pure tension. Broom reports that " experimental uncertainties were such that only general confirmation of theory was obtained."

The present experiment is a further attempt to observe the anisotropic changes in resistivity. It is clear from the previous work and from general considerations that certain conditions had to be fulfilled for decisive results:

1. Since recovery of resistivity occurs at " elevated" temperatures, the work has been done at sufficiently low temperatures to " freeze in" the defects.

2. The behavior of polycrystalline material is probably undesirable for a basic understanding of defect formation because of the inherent difficulties in analysing the results for aniso-

tropy as well as the more basic complication of interaction between crystallites of different orientation. Single crystals have been used.

3. The method of measurement of resistance should yield more or less direct results bearing on the question of anisotropy (i.e., a single experiment should give the desired information obviating the need of statistical analysis of several experiments).

4. The theoretical work for dislocation scattering has been done for elastically isotropic material. Among the metals tungsten is the best in this respect but, for experimental reasons, aluminum has been used. Aluminum is only slightly poorer than tungsten and is considerably better than copper in this respect.

5. It is desirable to work with a material which is initially electrically isotropic. This is true of cubic metals; aluminum is face - centered cubic.

CHAPTER III

EXPERIMENTAL PROCEDURE

The bulk of the experimental work was done on 99.99+ percent pure aluminum supplied by the Aluminum Corporation of America. Principle impurities were iron, copper, and silicon with traces of calcium and magnesium. Preparation of the samples follows a technique developed by Noggle[29]. Stock material in the form of 1-2 inch round rod or square bar was machined to the typical shape shown in figure 1. Since the geometry of the specimen is an important factor in the calculations, a careful machining schedule was followed.

1. Aluminum stock was cut to appropriate length, the ends faced and center-tapped.

2. The reduced section was turned to about 0.350 inches.

3. Flat faces were milled on the unreduced end poritons, the faces being 90° apart.

4. Setting the specimen down on its flat faces on a gauge block and using a vernier height marker, shallow lines were scribed 90° apart and parallel to the specimen axis. Thus a vector drawn from and normal to the specimen axis and through a scribe line defines the normal direction for a flat face.

5. Number 21 holes were drilled in the ends normal to the flat faces and centered on the scribe lines.

6. Two circles approximately one inch apart and centered on the reduced section were scribed so that the planes of the circles were normal to the specimen axis. This defines the gauge

length of the specimen.

7. Using a traveling stage microscope on a Tukon hardness machine, four indents were made along each of the four scribe lines and between the two circles. The first indent was 1/2 cm from a given circle; the following indents were 1/2 cm from each other.

8. Number 80 holes (0.0135 inches) were drilled, centered on the indents.

9. Pure aluminum wire, drawn to 0.014 inch diameter, were forced into the holes.

Following machining and a careful cleaning and etching, the specimen was inserted into the crucible as shown in figure 1. Using the Bridgeman[30] technique, single crystals were grown in a vacuum ($2 \times 10^{-}$ mm of Hg.) furnace. Following the casting, the specimen was etched. Assuming a single crystal had been obtained in the melt (efficiency was approximately 90 percent), the specimen was oriented by the Laue back reflection method. Inserting the square faces in a special holder, x-ray shots of two perpendicular faces were taken.

The ends of the specimen were next sawed off as shown in figure 1 with a jewelers' saw in such a manner that deformation was limited entirely to the region of cutting. The final step before an experimental run was a 12 hour vacuum furnace anneal(>600°C).

Pulling of the crystals was performed in a tensile machine designed and built in the laboratory prior to the initiation of the experiment. Basically the load is delivered to the specimen over a fulcrum using a variable lever arm. Actually the loading was accomplished by electrically driving either a 50 pound or 5 pound weight car away from the fulcrum. As the car traveled out applying

more load, elastic extension of the pulling system and plastic flow of the specimen caused the lever arm to fall slightly. This activated a switch turning on a "raising" motor which raised the fulcrum to compensate for the extensions.

The fulcrum was a carbide knife edge. One inch from this edge was another such edge, inverted from the first. A yoke swinging over this edge connected to a pull rod which transmitted the load to the specimen. To allow complete rotation of the specimen, universal joints were also included in the pulling system; the specimen was held by gimble joints for this purpose, also. The specimen was pin-loaded. The pull rod itself was 1-4 inch diameter steel tube of 0.020 inch wall thickness.

The machine was designed for operation at liquid helium temperature and above. For helium operations, the double Dewar flask technique was employed, liquid nitrogen in the outer flask and liquid helium in the inner one. To shield the liquid helium from above as well, a stainless steel can was mounted above the helium bath inside the inner flask. This can was filled with liquid nitrogen. The can was fixed to the table upon which the tensile machine was mounted.

The specimen was connected through a gimble joint to the center of a base plate, the bottom plate of a tripod arrangement. Connecting the tripod and the stainless steel can was a 3-16 inch wall thickness pyrex glass sleeve. Thus, while the pull rod, specimen, universal joints, and gimbles were under extension, the tripod, glass sleeve and stainless steel can were under compression.

The function of the glass sleeve, aside from transmitting load, was to form a buffer between the liquid helium in the inner

flask and the liquid nitrogen in the stainless steel can. Similarly, the pull rod was made of stainless steel because of its low thermal conductivity. The rod passed through a central port hole in the stainless steel can. To minimize heat leaks, the current carrying leads were passed through one of three eccentric port holes in the can. The other port holes carried the potential leads, thermocouples and the helium transfer tube.

Helium was transferred in a manner to permit maximum exchange in the initial filling by passing the cold helium vapor through the tripod to the base of the Dewar flask. To do this, the transfer tube was gently pushed into contact with a funnel connected to the tripod. For subsequent transfers, the transfer tube was lifted away from the funnel. In this way, the initial helium vapor, warm compared to the liquid below in the Dewar flask, was not passed through the liquid. To accumulate four liters of helium in the flask initially required approximately 7 1/2 liters.

Using either the 50 pound car or the 5 pound car offered a total applied load of 1000 pounds or 100 pounds respectively. Full load was applied in approximately 75 minutes. Load was directly recorded by counters geared to the fine-thread (40 threads per inch) screw drive of the loads cars. Head motion was read directly to 10^{-4} inches by a counter geared to the raising motor.

The procedure used in pulling the crystal and making measurements varied with the immediate purpose of the run. Typically the specimen was strained a given amount and resistance then measured, the specimen strained further and resistance remeasured. This sequence was possibly interrupted for a high temperature anneal.

These anneals were accomplished as follows. Assuming the

deformation was carried out at 4° K, to warm to 78° K one simply transferred liquid nitrogen into the inner dewar containing liquid helium. This caused the liquid helium to boil away quickly, leaving the dewar filled with liquid nitrogen. After a suitable period at 78° K, to return to 4° K a glass tube extended from the bottom of the inner flask through a port hole in the stainless steel can, and out the top of the flask. This tube connected to a 25 liter liquid nitrogen storage can which in turn was connected to a vacuum fore pump. In this manner the nitrogen was pumped out of the dewar into the storage can. When all but a slight bit of nitrogen was removed from the inner flask, liquid helium was transferred into the flask.

To anneal to room temperature, the Dewar system was removed from about the specimen. Returning to 4° K only required the reassembly and new transfer of helium.

For several specimens strained at liquid nitrogen temperature, the liquid nitrogen-room temperature range was explored by a nitrogen vapor technique which allowed the attainment and maintenance of a desired temperature to ± 1° C. A similar method has been described in the literature.

The resistance measurements were made by the IR drop method. That is, a known current of between 15 and 20 amperes was passed down the specimen and the drop in voltage between various sets of probes determined. A schematic diagram of the apparatus is shown in figure 2. Six volt storage batteries were the source of potential. Leakage currents and heating effects were searched for by varying the current level but found to be absent. Total heat dissipation in the specimen and current contacts was less than four milliwatts.

To compensate for contact and thermals EMFs, reading of potential drop was made with the direction of the current reversed. The stray EMF calculated by this procedure agreed very closely with the measured no-current potential.

Temperatures were measured by means of two copper-constantan thermocouples placed at the ends of the specimen. Readings from either thermocouple were reproducible in themselves although readings between thermocouples were different. Preliminary calibration showed these different readings were apparently due to different compositions in the thermocouples rather than different temperatures: no temperature gradients were observed.

CHAPTER IV

METHOD OF COMPUTATION

Before describing the methods of computation, it would be helpful to consider the problem involved. Assume the specimen has been given some extension. Following this extension, a current is passed axially through the specimen and voltage readings are made between any desired pair of potential probes. The problem is, then, how can these measurements be interpreted in terms of the components of electrical resistivity.

Under the usual experimental condition where one is interested only in some average value of resistivity, the analysis is simple. Presumably the potential probes are a distance l apart after extension and the cross-sectional area is A. These dimensions are related to the initial value of l_o and A_o by the obvious relations $l = \epsilon l_o$ and $A = A_o/\epsilon$. If V is the measured voltages and I is the current, we would have

$$\rho = \frac{RA}{l} = \frac{V}{I} \frac{A_o/\epsilon}{l_o\epsilon} = \frac{1}{\epsilon^2} \frac{V}{I} \frac{A_o}{l_o}$$

In the present experiment, the situation is more complicated. The relation $A = A_o/\epsilon$ still holds. For two potential probes rotated about the specimen with respect to each other, we can no longer write $l = \epsilon l_o$. Thus one problem to consider is that of geometry: knowing where the potential probes are with respect to each other initially, what are the new positions after some extension?

Furthermore, we can no longer write $\rho = RA/l = VA/I$ since we now are interested in all the components of the resisitivity

tensor. Instead it is necessary to make a more general calculation of the potential distribution in the specimen. This distribution will be some function of the components of resistivity. Having effectively determined the distribution of potential by sufficient voltage measurements on the specimen, we should be able to determine these components.

Since the analysis is somewhat complicated and since a small amount of arbitrariness is possible, the results for specimen 32 are treated in detail in the appendix.

We describe the geometry first. The description follows that of Schmid and Boas[31]. Two coordinate systems suggest themselves. These are shown in figure 3. The obvious one we may call the laboratory system. The coordinate axes of this system are defined by the specimen axis, taken as the z' -axis, and two other orthogonal directions. It is convenient to choose these as the direction of incidence of the x-ray beam when taking a Laue shot (x') and the third orthogonal direction (y'). With this choice of axis, all the potential leads at the beginning of the experiment lie either on the x'-axis or the y'-axis.

The other coordinate system chosen reflects the fact that all of the experimental runs were made using crystals which deformed in single slip throughout the run. These coordinate axes are the slip direction--the y-axis $(1\bar{1}0)$, the normal to the slip plane--the z-axis (111), and the third orthogonal direction--the x-axis $(11\bar{2})$. The relationship between the two systems is shown in figures 3 and 4 with the pertinent angles also indicated.

To follow the motion of lattice points under elongation, consider figure 4. Quantities before deformation have the subscript o;

following deformation, ϵ . Since the deformation is a pure shear in the direction y of a magnitude $\underline{a}$, each P_o (x_o, y_o, z_o) transforms into the point P_ϵ $(x_\epsilon, y_\epsilon, z_\epsilon)$ by glide in the y-direction. Thus the transformation is

$$x_\epsilon = x_o$$
$$y_\epsilon = y_o + az_o$$
$$z_\epsilon = z_o$$

Also for the line elements of P_o and P_ϵ we have

$$l_o^2 = x_o^2 + y_o^2 + z_o^2 \qquad l_\epsilon^2 = x_\epsilon^2 + y_\epsilon^2 + z_\epsilon^2$$

$$y_o = l_o \cos \lambda_o \qquad y_\epsilon = l_\epsilon \cos \lambda_\epsilon$$

$$z_o = l_o \sin \chi_o \qquad z_\epsilon = l_\epsilon \sin \chi_\epsilon$$

Combining equations it follows that

$$(l_\epsilon/l_o)^2 = \frac{x_\epsilon^2 + y_\epsilon^2 + z_\epsilon^2}{l_o^2} = \frac{l_o^2 + 2ay_oz_o + a^2 z_o^2}{l_o^2}$$

or $(l_\epsilon/l_o)^2 = 1 + 2a \sin \chi_o \cos \lambda_o + a^2 \sin^2 \chi_o$

Solving for $\underline{a}$,

$$a = \frac{1}{\sin \chi_o} \left[\epsilon^2 - \sin^2 \lambda_o\right] - \cos \lambda_o \quad \text{where } \epsilon = l_\epsilon/l_o$$

In a better form for computation

$$a = \frac{\cos \lambda_\epsilon}{\sin \chi_\epsilon} - \frac{\cos \lambda_o}{\sin \chi_o}$$

From the diagram it is obvious that $l_o \sin \lambda_o = l_\epsilon \sin \lambda_\epsilon$ and, since $z_\epsilon = a z_o$, $l_\epsilon \sin \chi_\epsilon = l_o \sin \chi_o$

we have $\epsilon = \frac{l_\epsilon}{l_o} = \frac{\sin \lambda_o}{\sin \lambda_\epsilon} = \frac{\sin \chi_o}{\sin \chi_\epsilon}$

It has been well verified that volume is conserved in plastic flow.(Thus we may write for the new cross-sectional area A in terms of the old A_o,

$$A_\epsilon = A_o/\epsilon$$

This essentially concludes the problem of geometry. The problem of finding the potential distribution may be solved as follows:

Let $\vec{j} = \sigma \vec{E}$ or $\vec{E} = \rho \vec{j}$

where $\vec{j}$ is the electrical current density, $\vec{E}$ is the electrical field, σ is the electrical conductivity and ρ is the electrical resistivity. Since $\vec{j}$ and $\vec{E}$ are vectors, σ and ρ are second rank tensors. The equation of continuity is $\operatorname{div} \vec{j} + \partial\rho/\partial t = 0$. Assuming a steady state, ρ is not a function of time, $\partial\rho/\partial t = 0$ and

$$\operatorname{div} \vec{j} = 0$$

Also $\vec{E} = -\operatorname{grad} \phi$ where ϕ is the electrical potential.

Thus $\operatorname{div} [\sigma \operatorname{grad} \phi] = 0$

This is the second order differential equation to be solved. The boundary conditions are

$$\int_{\text{end}} \vec{j} \cdot d\vec{A} = I \qquad \text{and} \qquad j_n = 0$$

on the surface of the cylinder. A is the cross-sectional area of the cylinder and j_n is the component of current density normal to the surface of the cylinder. I is the total current.

The differential equation for ϕ can be solved rigorously. Following Maxwell, we may take σ to be a symmetric tensor. However, we are more particularly concerned with the values of the principal axes of σ or ρ. Following Sondheimer and Mackenzie[4], we take the coordinate axes of the slip system to be the directions

of the principal axes. It seems clear from symmetry considerations that these should be the principal axes for a system in single slip. It is also necessary to assume ρ or σ are not functions of position.

Under these assumptions and working in the slip coordinate system, we have $\sigma_x \frac{\partial^2 \phi}{\partial x^2} + \sigma_y \frac{\partial^2 \phi}{\partial y^2} + \sigma_z \frac{\partial^2 \phi}{\partial z^2} = \frac{1}{\rho_x} \frac{\partial^2 \phi}{\partial x^2} + \frac{1}{\rho_y} \frac{\partial^2 \phi}{\partial y^2} + \frac{1}{\rho_z} \frac{\partial^2 \phi}{\partial z^2} = 0$

where $\sigma = \begin{pmatrix} \sigma_x & 0 & 0 \\ 0 & \sigma_y & 0 \\ 0 & 0 & \sigma_z \end{pmatrix}$, $\rho = \begin{pmatrix} \rho_x & 0 & 0 \\ 0 & \rho_y & 0 \\ 0 & 0 & \rho_z \end{pmatrix}$

The solution to the differential equation is

$$\phi = Fx + Gy + Hz + K$$

with $|\vec{j}| = j_z$ where F, G, H, and K are constants.

Therefore the current density is everywhere parallel to the specimen axis. It is obvious that this solution satisfies the differential equation and the boundary condition.

To evaluate the constants, we see that

$$E_x = -\partial\phi/\partial x = -F = \rho_x j_x \,, \qquad \text{etc.}$$

$$\therefore \phi = \rho_x j_x x + \rho_y j_y y + \rho_z j_z z + K$$

Since the current density is axial,

$$j_x = |j| \cos(\angle x z') = \frac{I}{A} \cos(\angle x z'), \qquad \text{etc.}$$

Finally, since we are only interested in differences in potential,

$$\Delta\phi = \frac{I}{A}\left[\rho_x \Delta x \cos(\angle x z') + \rho_y \Delta y \cos(\angle y z') + \rho_z \Delta z \cos(\angle z z')\right].$$

Or, in terms of the angles used in figure 4,

$$\Delta\phi = \frac{I}{A}\left[\rho_x \Delta x \cos\phi + \rho_y \Delta y \cos\lambda + \rho_z \Delta z \cos\chi\right]$$

In the remainder of the work $\Delta\phi/I$ is called the resistance R.

The manner in which these calculations are used is shown in the appendix where the data pertaining to specimen 32 are treated.

CHAPTER IV

DISCUSSION OF ACCURACY

It has been stated previously that the cold-working should be done at a sufficiently low temperature to "freeze in" all the deformation products. It is shown here that some annealing does occur below liquid nitrogen temperature. This is a primary reason for extending the research to liquid helium temperature.

In analysing the data, it is implicitly assumed that Matthiessen's[33] rule is obeyed. This rule states that the resistivity, ρ, can be broken up into two parts: a temperature dependent part, ρ_t, and a temperature independent part, ρ_r, the residual resistivity. Furthermore the rule states that crystal defects affect only ρ_r. This has been shown to be the case for small impurity content in a pure metal.

It is generally believed that Matthiessen's rule is also obeyed for small deformation. There have been reports for and against the application of the rule to cold work[34-39]. However, the recent work of Boas and Nicholas[40] seems to indicate that the rule holds for pure materials but not for alloys. Some testing of it was done in the present research and no clear deviations were seen. However, it seems desirable to circumvent this controversy. If Matthiessen's rule does not hold, phonon interaction with mechanical defects should be the main cause. For this reason, as well as attempting to avoid temperature correction, the measurements have been made at 4°K.

There is also a more important reason for measuring ρ in helium. If we were content to measure an average resistivity, we could write $R = \frac{\rho l}{A} = \frac{\rho l^2}{V}$ where l is the distance between potential probes, A is the cross-sectional area, and V is the volume. Since volume is conserved,

$$\rho_\epsilon/\rho_0 = \frac{R_\epsilon V}{l_\epsilon^2} \cdot \frac{l_0^2}{R_0 V} = \frac{1}{\epsilon^2} \frac{R_\epsilon}{R_0}$$

or,

$$\Delta\rho/\rho_0 = \frac{\rho_\epsilon - \rho_0}{\rho_0} = \frac{1}{\epsilon^2} \frac{R_\epsilon}{R_0} - 1$$

Thus an accurate determination of ϵ is necessary unless $R_\epsilon >> R_0$. This is only the case at 4°K. For this reason, no reproducible results were obtained of anisotropy for measurements at 78°K.

The results obtained from measurements at 4°K concerning anisotropy are listed in Tables I-III. To illustrate the handling of the data, a portion of the data related to specimen 32 is presented in detail in the appendix.

Since a cubic metal is initially electrically isotropic, all combinations of potential probes should have given the same average resistivity. This was not observed. However microscope examination showed shifting of the leads with respect to each other axially. This is presumably a combination of error in drilling and an actual shift in melting. To minimize this error, the axial distance ($\Delta z'$) were adjusted so that the measured value of resistance between probes at 0°C agreed with the adjusted $\Delta z'$. In no case did the adjustment exceed the wire diameter.

Following elongation of a specimen, the calculated new positions of the leads were compared with those observed in a microscope. (Actually the positions measured and observed were the axial component, $\Delta z'$, of the separation of two leads often not on the same

face.) A typical set of the data is given in Table V. The agreement is certainly better than 2 o/o. This in itself confirms the accuracy of the single-slip geometry analysis since the microscope readings involve considerable error.

The analysis of the data presents one peculiar difficulty. It will be noted that the contribution of a resistivity component to the actual resistance reading is weighted with an angular cosine dependence as well as lead separation. It would have been very desirable to place potential probes at particular positions so that the resistance reading gave the desired resistivity component directly. Technically this is quite impossible. In fact, theoretically it is always impossible to fix stationary probes to define the normal to the slip plane direction and, with the exception of one unique orientation, to define the x-direction. Only the slip direction could be permanently defined by a fixed set of stationery probes. Thus a more feasible arrangement was chosen.

Since current is passed axially through the specimen, it is an unfortunate fact that $\cos(\angle xx')$ is always much smaller than the other cosines. The x-direction is always close to the horizontal for a vertical current flow. To aggrevate the matter, $\cos(\angle xx')$ becomes smaller with slip. This has the effect of introducing a large amount of error in ρ_x. To minimise this error, an attempt was made to choose orientations yielding as large a value of $\cos(\angle xx')$ as possible, as well as representing crystals which remained well out of the double slip region of the unit stereographic triangle. For this reason, $\cos(\angle xx')$ is shown for each specimen in Tables I-III. For comparison, $\cos(\angle yx') \simeq \cos(\angle zx') \simeq 0.7$. It is easy to see that the results for specimen 33, which represents an

almost ideal orientation in these respects, are much more consistent than the others in its values of ρ_x, although not completely so (ρ_x goes up slightly after the first anneal). The values of ρ_x must be regarded as the most poorly determined experimental quantity.

It is difficult to calculate the error in the anisotropy data. An estimate of the error in the absolute value of the resistivity was made as follows. Having derived the best values of resistivity by the methods shown in the appendix, these values are taken and inserted back into the equation for a particular set of leads. The equations are of the form

$$\cos(\angle xx')\Delta x\rho_x + \cos(\angle yx')\Delta y\rho_y + \cos(\angle zx')\Delta z\rho_z = R\Delta$$

Substituting calculated values of resistivity components on the left side allows a comparison with the measured resistance shown in the right side. The disagreement between values serves as an excellent index of error since the error here is accumulated from all sources such as inaccuracy in position of probes, x-ray orientation, strain and resistances measurements. The errors here are about 2 to 2 1/2 o/o. This will imply different errors in the determination of the various components for the reasons stated above. For ρ_y and ρ_z an error under 1 o/o is implied. The errors in ρ_x can extend to much greater values, perhaps to 15 o/o.

However, the error of interest is not in the absolute value but in the differences of resistivity such as those before deformation and those following extension. The magnitude of the errors involved in the differences will vary with the magnitude of the difference, being largest for small differences. A fair estimate of accuracy seems to be about 10 o/o for strains less than 6 o/o

to about 5 o/o for the larger strains. This is the case for ρ_y and ρ_z. In the case of ρ_x the corresponding errors were 50 o/o and 20 o/o. On comparing different specimens, no systematic trend is observed from the conclusions to be drawn concerning anisotropy.

CHAPTER V

EXPERIMENTAL RESULTS

From Tables I-III we may conclude the following: within the stated error, the changes in resistivity due to deformation and annealing are isotropic. This simple statement should be regarded as the primary result of this research.

Besides this statement of complete isotropy, it is possible to make several other more or less definite ones.

1. Referring to Table IV, we see that approximately 10 o/o of the resistivity increase anneals between 4°K and 78°K; of the remainder, approximately 65 o/o anneals between 78°K and 300°K. This last anneal represents about 55 o/o of the total resistivity change. Probably more important than these figures is the tendency for larger annealing to occur with larger strain, although the tendency is small.

2. The increment of resistivity is larger for specimen 31 strained at 4°K and annealed at 78°K than for specimen 32 strained at 78°K despite the fact that 32 received a larger extension than 31. This difficulty disappears, however, when the resistivity increments are compared with the stress rather than the strains. Here we have the expected association that the larger resistivity increment is associated with the larger stress.

3. Figure 5 represents a plot of $\Delta\rho$ vs. ϵ^2. It is seen that the curve is linear. Since, as discussed below, the stress-strain curve is also linear, $\Delta\rho \propto \sigma^2$

4. The behavior of the stress-strain curve depends sharply

on temperature.

a. The curve is linear in the range investigated for extensions at 4°K, as shown in figure 6. If the strained sample is annealed to 300°K and restrained at 4°K, a distinct upper yield point phenomenon is present. An examination of figure 7, which is a magnification of figure 6 in the region of the upper yield point, discloses that there is annealing of the curve as well. However, the magnitude of the yield point is so large that an additional stress above the final stress in the first load is needed in the reloading to reinitiate plastic flow. At first glance it would appear that there had been no annealing, but comparing the reloading curve with the original loading curve shows a characteristic anneal.

b. The curve is parabolic for extension at 78°K as shown in figure 8. If the sample is annealed at 300°K and re strained at 78°K, appreciable annealing occurs and a slight yield point is observed. No detailed examination was made of relative magnitudes of yield points but some idea can be gained from the fact that yield points at 78°K went unnoticed until the large yield point at 4°K was noted. To explore the magnitudes further, head motion observations were made and compared with self-recording measurements of applied load. The yield phenomenon showed itself in both cases. These measurements confirm the relative magnitudes stated above.

It is also interesting to note that the yield point was also present on specimens pulled at 78°K and given a rest

period at 78°K. The magnitude increased as the length of the rest period was increased, as one would expect.

Figure 8 also shows the enhanced annealing when the specimen was taken to 550°K between loading at 78°K.

c. The curve is parabolic for extensions at 300°K as is shown in figure 9. Reloading after a rest period shows annealing but no yield point is detected.

d. Specimen 34, pulled at 4°K, warmed to 78°K and pulled further at 78°K failed to show the yield point. Unfortunately there is some doubt in this result due to experimental difficulties. After this specimen was given an additional rest period at 78°K, the yield point of the usual magnitude was observed. Warming to room temperature and straining further at 78°K again showed the yield point. Warming to room temperature and pulling still further at room temperature failed to show the yield point.

5. Considerable effort was made in an effort to observe the temperature ranges of the resistivity anneals. It was simple to find the higher anneal. This was observed to occur in the range of -100°C although the "exact" temperature depended on the strain (or stress) level. Annealing was observed over the entire range from -80°C to -120°C, beginning at lower temperatures for higher strain levels.

6. Prompted by the statement from Manintveld that annealing also occurs for the resistivity in aluminum at liquid nitrogen temperature, an effort was made to observe this. Under ordinary conditions, no such recovery was found. Believing that the process of recovery may have been occurring too rapidly to be detected by

our relatively slow methods, an attempt was made to load instantaneously and follow a possible resistivity decay. Taking resistivity measurements after extensions of the order of 30 o/o only two minutes after initiating deformation and continuing for an hour or two still failed to show this annealing. It is believed that the annealing of resistivity found between 4°K and 78°K corresponds to that of Manintveld although it is not simple to explain the discrepancy.

Since the basic purpose of this research was to measure electrical resistivity, the measurements of the stress-strain behavior were somewhat incidental though considerable effort was made in this direction also. However, it is obvious from this catalog of observations made above that considerable more work remains to get a truly consistent picture. Some of the observations made were made only once, others several times. Some measurements (such as the behavior of a sample strained at 4°K, annealed to 78°K, and strained further at 4°K) were not even made. Having shown that the resistivity changes are isotropic, it will be much simpler and more economical in the future to pursue stress-strain behavior with less of the tedious precautions required by anisotropy measurements.

CHAPTER VII

DISCUSSION OF RESULTS

The complete isotropy of resistivity found in this research is an unexpected result. It is impossible to fully explain this result at the present time but we may list some possible explanations.

1. The scattering of electrons by dislocations is negligible. This may be due to a low density of dislocation or a low scattering cross-section per dislocation length. The latter possibility would confirm the calculation of magnitude given by Dexter and Hunter and Nabarro. The resistivity changes are then due to interstitials, cacancies, etc.

2. The calculation of anisotropy for screw and edge components are incorrect. This does not seem likely for, although the numbers may be incorrect, it seems clear that some anisotropy is to be expected.

3. The array of dislocations laid down is isotropic. This is contrary to the intent of the experiment since work has been limited to the single slip region. Since there exists a distribution of dislocations lengths, one would expect some multiplication on inactive slip planes but it is difficult to account in this way for the relatively large changes observed.

To make these comments more quantitative, assume that microscopic slip will start on the latent slip plane when the resolved shear stress in that plane is equal to the yield stress. Take the critical yield stress to be ~ 100 gm/mm2 at $4^{\circ}K$, although it is

actually higher. Referring to a standard projection of the crystal orientation of specimen 33, it is found that, for the latent system,

ψ_2 = (slip plane normal and specimen axis) $\simeq 85^\circ$

λ_2 = (slip direction and specimen axis) $\simeq 20^\circ$

But σ (resolved) = σ (axial) $\cos \psi_2 \cos \lambda_2$ for the latent slip plane.

$\cos \psi_2 \cos \lambda_2 < 1/3 \times 10^{-1}$

$\therefore \sigma$ (axial) $> 30\, \sigma$ (resolved) $\simeq 4.5 \times 10^2$ lb/in^2

Since the area of the specimen is about 1/8 in^2, a load of considerably more than 500 pounds would be required to initiate dislocation generation on the inactive plane. Furthermore, since the calculation has been somewhat biased towards a low estimate of the critical stress and since no account has been taken of hardening effect of the active slip plane, which would also raise the critical stress for the inactive system, it seems reasonable to assume a negligible amount of cross-slip throughout the entire experimental run with maximum load of 750 pounds. It can be reported that no evidence for cross-slip was evident on the surface of the specimen after the run and even after some further extension. Also the excellent agreement between measured and calculated positions of potential probes points to solely single slip since the calculations assume this. It should be noted that 3 percent extension was achieved with 220 pounds applied; these measurements showed isotropy in ρ_y and ρ_z to $\pm$ 2 o/o.

In attempting to explain the behavior of the crystal in terms of particular defects, it is essential to compare the results obtained here with past results. One of the most comforting conclusions that is quite clear in this way is that, with the exception

of the anisotropy results which are essentially the first obtainable, all the results of this research on aluminum are similar to those obtained by Blewitt and Pry and Hennig on copper. At the risk of oversimplification, one might propose that aluminum and copper are the "same" metal, but with shifted characteristic temperatures.

Realizing that two such metals do not provide a sufficient test for these remarks, it is nevertheless tempting to draw the conclusion that the results of deformation in a metal are rather gross distortions of the lattice. The particular electronic structure of the metal atom and other such detailed characteristics seem to be of lesser importance. This is, of course, in general agreement with the concept of dislocations, vacancies and interstitials. It would be very desirable to compare the behavior of these face-centered cubic metals with other structures such as hexagonal metals (e.g., zinc).

As was stated in the preliminary discussion, the annealing behavior in cold-worked and irradiated copper seems to be the same in the range of -20°C. Since dislocations are not expected to anneal below room temperature in copper, one is tempted to identify this anneal with a defect such as vacancies. The present data seem to fit into this picture very well. However, there is one disturbing feature present. The corresponding annealing in aluminum reduces the mechanical strength. In copper, the mechanical strength is not annealed until about 100°C. Presumably in aluminum the two annealing processes are not resolved. The fact that the resistance recovery in aluminum occurring between -120°C and room temperature is spread out over a range of temperature again points toward dislocation annealing.

It is also important to remember that the resistance changes produced by irradiation are large, indicating that point defects are effective scatterers or that an extremely large number are produced.

Still another piece of evidence bearing on this subject is the results of the quenching experiments of Koehler and Kauffman[41]. They quenched heated gold wires from temperatures such as 800°C to liquid nitrogen and find a substantial resistivity increase. Since the concentration of vacancies is far greater than that of other point defects at high temperatures, it is believed that they have succeeded in quenching vacancies. Their investigation shows mobility of vacancies at -20°C. It would be very interesting to see the effect of these vacancies on the yield stress.

On the basis of these remarks, it seems possible to conclude tentatively that the -100°C anneal in aluminum corresponds to vacancies and dislocations simultaneously annealing. In copper, one would expect these to be resolved, as earlier suggested. Resistivity-wise, the effect of vacancies overwhelms that of dislocation so that the recovery appears isotropic in aluminum. It is possible that, if one can succeed in making an accurate investigation of possible resistivity anisotropy at very low strain levels, the annealing in the range of -120°C to -80°C could be resolved into two steps. The outlook for such resolution using the methods of this experiment are not encouraging since present accuracy and sensitivity are not sufficient.

Possible sources for vacancies (and interstitials) in cold-working have been suggested and widely discussed recently[42,43]. An effective source seems to be the crossing of screw dislocations. When a moving screw on the active slip plane crosses a screw in

latent plane, a line of vacancies or interstitials should be left behind, depending on the signs of the two dislocations.

It would be very convenient to explain the data on the basis of the following sort of model. If it is assumed that a trail of vacancies is left behind when an expanding Frank-Read loop crosses a screw dislocation, that about 1 ev. is required to create such a vacancy and that the shape of the loop retains the form of a circle, one finds $\Delta\rho \propto \epsilon^{3/2}$, as van Beuren has calculated.

However, there is room for criticism here. Since the screw component of the loop is the one concerned with vacancy production, one would expect this portion of the loop not to move as far as the edge component through a network of intersecting dislocations. This is in agreement with the recent observations of Chen and Pond[44] that slip bands in aluminum grow more slowly in the direction perpendicular to the active slip direction than in the slip direction. Using this idea, one would expect the shape of the loop to resemble an ellipse more than a circle.

Consider a loop with Burger's vector in the y-direction. We expect the loop to become an ellipse with its major axis along the y-direction, its minor axis along the x-direction. Focussing our attention on the part of the ellipse which is primarily screw, let N be the density of screw dislocations crossing the slip plane, a be the atomic separation of atoms, E the energy to form a vacancy and σ the applied stress. The number of trails of vacancies formed in expanding the loop to an ellipse of semi-minor axis x per unit length in the y-direction in the predominantly screw portion is approximately Nx. To expand the ellipse a distance dx along the x-direction requires an energy per cm of $\frac{Nxdx\sigma E}{a}$. The work done by the

stress field is σ a dx. Thus the ellipse expands to a critical distance $x_c = \frac{\sigma a^2}{NE}$.

Consider now the portion which is primarily edge-type in nature. The force on an incremental length, ds, is $\sigma a\, ds = \sigma a R\, d\theta$ where R is the radius of curvature and $d\theta$ is the corresponding incremental arc. The line tension is approximately $\frac{Ga}{2} d\theta$. Thus the critical radius of curvature is $R_c = \frac{Ga}{2\sigma}$.

Now, from calculus, $R = \left[1+\left(\frac{dy}{dx}\right)^2\right]^{3/2} \Big/ \left|\frac{d^2y}{dx^2}\right|$. If our elipse is given by $\frac{x^2}{x_c^2} + \frac{y^2}{y_c^2} = 1$, we find $R = \frac{\left[x_c^4 y^2 + y_c^4 x^2\right]^{3/2}}{x_c^4\ y_c^4}$. We evaluate the radius of curvature when $x = o$ and $y = y_c$. Then $R_c = \frac{x_c^2}{y_c}$. Therefore $y_c = \frac{x_c^2}{R_c}$. Since $x_c \propto \sigma$ and $R_c \sim 1/\sigma$, we have $y_c \propto \sigma^3$. This would say that the edge portion moves much further than the screw portion.

We should also calculate the resistivity increase due to vacancies. The number of vacancies per ellipse is of the order of

$$n \approx \frac{1}{2} \int_0^{x_c} \ell y_c N x \frac{dx}{a} = \frac{N}{2a} x_c^2 y_c$$

Assuming the resistivity increase to be proportional to the number of vacancies, we have $\Delta\rho \propto x_c^2 y_c \propto \sigma^5$

This certainly is not in agreement with experiment. Consider however, the magnitude of the critical distances

$$y_c = \frac{\sigma^2 a^4}{N^2 E^2} \cdot \frac{2\sigma}{Ga} = \frac{2\sigma^3 a^3}{GN^2E^2}$$

Recent work indicates that, for good single crystals, N is less than 5x10 lines/cm. We shall take a value of shear stress corresponding to the applied load of 750 pounds for specimen 33. Taking E = 1ev = 1.6×10^{-12}, N = 5×10^{2} lines/cm^2, $\sigma = 2\times10^{8}$ dynes/cm^2

$a = 2\times10^{-8}$ cm. and $\sigma = 5\times10^{11}$ dynes/cm^2, we get $y_c \approx 10$ cm., $x_c \approx 2\times10^{-2}$ cm. Whereas the value of x_c is reasonable, y_c indicates that the loop has run out of the crystal in this direction.

This suggests how the model should be modified. We shall, instead, assume that, for some small value of stress depending on the correct value of N, the edge component of the loop runs out of the crystal. It is conceivable that the yield stress alone is enough to cause this, since, at the present stage of knowledge, N may well be considerably smaller than the value assumed here.

There are some experimental observations to support such a model. Chen and Pond[44] have examined the formation of slip bands, comparing the rates of formation of the band in the slip direction and normal to it. They found the band to form faster in the normal direction, indicating the emergence of the edge component. It would be interesting to have quantitative data on rate of formation as function of direction under constant stress rate.

Wu and Smoluchowski[45] have found a breakdown of Schmid's resolved shear stress law for very thin specimens. They used pure aluminum sheet material with cross-sectional dimensions of 0.2 mm. The direction of slip was then controlled by the direction offering least glide necessary to reach the surface as well as the resolved shear stress. This again indicates that slip depends heavily on the ability of a loop to reach the surface. If this is true, macroscopic strain should be largely accounted for by surface slip lines. It would be very desirable to have a "census" of slip lines to see how much the strain can be accounted for in this way.

It is also possible that the differences concerning the correct picture of slip lines between Heidenreich and Shockley[46] and

Kuhlmann-Wilsdorf and Wilsdorf[47] will be resolved by a size-effect. It would be desirable to see if the yield strength depends on size in this manner.

Having assumed that the edge component runs to the surface for very small stress, we now have y_c = the radius of the specimen except for small stress. Thus, again except for small stress,

$$\Delta\rho \propto \chi_c^2 \propto \sigma^2 \qquad \epsilon \propto \text{area of loop} \propto \chi_c \propto \sigma$$

These are just the dependences experimentally observed. This agreement may vanish if piling up of dislocations is considered. To make the calculations more quantitative more information is needed.

1. How many sources are active? This should be determined from future slip line study.

2. How many loops does a given source send forth? This will be controlled by the back-stress of the previous loops on the source as well as the number of obstacles cluttering the slip plane due to the motion of previous loops.

3. What is the "exact" shape of the loop? The ellipse used here is probably only a reasonable approximation.

4. What role does temperature play? Is it a diffusion of vacancies out of the slip plane? Can this account for the linear stress-strain curve at low temperature, the parabolic one at higher temperature?

The aging phenomenon found at low temperatures is interesting in itself. Since the aluminum is high purity (and the copper used by Blewitt and Pry and Hennig even more pure), it would seem to rule out the possibility of this being an impurity effect. However, since the yield point is a phenomenon most sensitive to the length of the longer dislocation lengths, it should take but a

TABLE I

SPECIMEN 31
$\cos(\angle xz') = 0.145$

	$\mu\Omega$cm x 10^3			
ϵ	ρ_x	ρ_y	ρ_z	Remarks
1.0	6.78	6.17	6.49	As-grown specimen
1.09	8.22	9.19	9.51	Pulled to 9 o/o elongation at 4° K
1.15	13.80	14.89	13.64	Pulled to 15 o/o elongation at 4° K
1.15	13.03	13.35	12.95	Annealed at 78°K over night
1.15	8.72	8.78	9.05	Annealed at 300°K for two weeks

TABLE II

SPECIMEN 33
cos (∠ xz') = 0.37

ϵ	ρ_x	ρ_y	ρ_z	Remarks
	— $\mu\Omega$ cm x 10^3 —			
1.0	7.10	7.03	7.05	As-grown specimen
1.03	8.01	7.46	7.53	Pulled to 3 o/o elongation at 4°K
1.09	10.62	10.42	10.85	Pulled to 9 o/o elongation at 4°K
1.09	10.79	10.05	10.26	Annealed at 78°K over night
1.09	8.78	8.10	8.27	Annealed at 300°K for four days
1.13	12.42	11.74	12.02	Pulled further at 4°K

TABLE III

SPECIMEN 32
$\cos(\angle xz') = 0.11$

ϵ	ρ_x ($\mu\Omega$cm $\times 10^3$)	ρ_y ($\mu\Omega$cm $\times 10^3$)	ρ_z ($\mu\Omega$cm $\times 10^3$)	Remarks
1.0	7.76	7.91	7.68	As-grown specimen
1.16	8.60	13.54	12.96	Pulled to 16 o/o elongation at 78°K
1.16	10.32	9.37	9.17	Annealed to 300°K for three days

TABLE IV

AVERAGE RESISTIVITY BEHAVIOR

Specimen	ϵ	ρ_4	ρ_f	ρ_{78}	ρ_{300}	$\frac{\rho_{78}-\rho_4}{\rho_f-\rho_4}$ (%)	$\frac{\rho_{300}-\rho_{78}}{\rho_{78}-\rho_4}$ (%)	$\frac{\rho_{300}-\rho_{78}}{\rho_f-\rho_4}$ (%)
		$\mu\Omega$ cm x 10^{-3}						
33	1.09	7.05	10.62	10.27	8.35	10	60	54
31	1.15	6.40	14.44	13.20	8.86	16	64	54
32	1.16	7.68	—	13.29	9.32	—	72	—

Note: $(\epsilon - 1) \times 100$ = percent elongation

ρ_4 = resistivity of undeformed crystal measured at $4^{\circ}K$

ρ_f = resistivity of deformed crystal, deformed and measured at $4^{\circ}K$

ρ_{78} = resistivity of deformed crystals measured at $4^{\circ}K$. Specimen 33 and 31 were deformed at $4^{\circ}K$, warmed to $78^{\circ}K$. Specimen 32 was deformed at $78^{\circ}K$

ρ_{300} = resistivity of deformed crystals measured at $4^{\circ}K$ after warming to $300^{\circ}K$

TABLE V

SPECIMEN 22

Lead Numbers	Axial Separation (cm.) Computed	Measured
7 - 14	0.485	0.479 - 0.496
9 - 15	1.434	1.375 - 1.381
2 - 12	1.210	1.257 - 1.263
10 - 8	1.257	1.228 - 1.234
5 - 16	2.118	2.081 - 2.093
1 - 16	1.983	1.956 - 1.962
1 - 8	1.821	1.840 - 1.834
9 - 12	1.926	1.934

BIBLIOGRAPHY

1. T. Broom, Adv. in Phys., 3, 27 (1954)
2. F. Seitz, Imperfections in Nearly Perfect Crystals (New York: Wiley)
3. J. S. Koehler, Phys. Rev., 75, 106 (1949)
4. J. K. MacKenzie and E. H. Sondheimer, Phys. Rev., 77, 264 (1950)
5. R. Landauer, Phys. Rev., 82, 520 (1951)
6. R. Hirone and K. Adachi, Schi. Reg. Res. Inst. Tohoku Univ. A, 3, 454 (1951)
7. D. L. Dexter, Phys. Rev., 86, 770 (1952)
8. A. W. Saenz, Phys. Rev., 91, 1142 (1953)
9. S. C. Hunter and F. R. N. Nabarro, unpublished (see ref. 1.)
10. J. S. Koehler, Phys. Rev., 60, 398 (1941)
11. P. G. Klemens, Aust. J. Phys., 6, 122 (1953)
12. D. L. Dexter, Phys. Rev., 87, 768 (1952)
13. P. Jongenburger, Phys. Rev., 90, 710 (1953)
14. F. Seitz, Adv. in Phys., 1, 43 (1950)
15. H. B. Huntington, Phys. Rev. 61, 315 (1942)
16. H. B. Huntington, Phys. Rev., 61, 325 (1942)
17. J. H. Bartlett and G. J. Dienes, Phys. Rev., 89, 848 (1953)
18. J. Molenaar and W. H. Aarts, Nature, Lond., 166 (690) 1950
19. M. J. Druyvesteyn and J. A. Manintveld, Nature, Lond., 168, 868 (1951)
20. J. A. Manintveld, Nature, Lond., 169, 623 (1952)
21. T. H. Blewitt, J. K. Redman, and F. A.Sherill, Phys. Rev., 91, 236 (1953)
22. R. R. Eggleston, J. Appl. Phys. 23, 1400 (1952)
23. A. W. Overhauser, Phys. Rev., 90 393 (1953)

24. H. Weyerer, Zeit. Metall. 44, 51 (1953)

25. H. G. van Beuren, Acta. Met., 1, 532 (1953)

26. R. H. Pry and R. W. Hennig, Acta Met., 2 (2) (1954)

27. T. Broom, Phil. Mag., 42, 56 (1952); Aust. J. Sci. Res. A. 5, 128 (1952).

28. T. Broom and W. K. Clothier, Aust. J. Sci. Res. A. 5, 119 (1952)

29. T. S. Noggle, Rev. Sci. Inst., 24, 184 (1953)

30. P. W. Bridgeman, Proc.Amer. Acad. Arts. Sci., 60, 305 (1925)

31. E. Schmid and W. Boas, Plasticity of Crystals (F. A. Hughes Co., London, 1950)

32. D. Hanson and M. A. Wheeler, J. Inst. of Metals, 45, 229 (1931)

33. A. Matthiessen, Rep. British Assoc., 32, 144 (1862)

34. C. W. Berhout, Physica, 18, 587 (1952)

35. J. W. Rutter and J. Reekie, Phys. Rev., 78, 70 (1950)

36. E. Bowen, R. R. Eggleston and R. H. Kropschot, J. Appl. Phys., 23, 630 (1952)

37. W. Geiss and J. A. M. van Liempt, Zeit. Physik, 41, 867 (1927)

38. M. Masima and G. Sachs, Zeit Physik, 51, 321 (1928)

39. K. Lucke, Zeit. Metall., 42, 1, (1951)

40. W. Boas and J. F. Nicholas, Aust. J. Phys. 6, 116, (1953)

41. J. W. Kauffman and J. S. Koehler, Phys. Rev. 88, 149 (1952)

42. A. H. Cottrell, Dislocations and Plastic Flow in Crystals (Clarendon Press, 1953)

43. W. T. Read, Jr., Dislocations in Crystals (McGraw-Hill, 1953)

44. N. K. Chen and R. B. Pond, J. Metals, 4, 1085 (1952)

45. T. L. Wu and R. Smoluchowski, Phys. Rev. 78, 468 (1950)

46. R. D. Heidenreich and W. J. Shockley, J. Appl. Phys., 18, 1029 (1947)

47. K. Wilsdorf and D. Kuhlmann-Wilsdorf, Z. angew. Phys., 4, 361 409, 418 (1952)

48. J. Washburn, K. Kennedy, L. O. Seaborn and E. R. Parker, Tech. Rep. 2, Ser. 27 (1951)

49. E. I. Salkovitz and J. S. Koehler, Acta Met., 1, 562, (1953)

50. P. Haasen, Doctoral Dissertation, U. of Goettingen (1953)

APPENDIX I

SAMPLE ANALYSIS OF SPECIMEN 32

Leads	$\Delta x'$ cm	$\Delta y'$ cm	$\Delta z'$ cm	$(R/\bar{R})$ 300°K	$\Delta z'$ (corrected) cm
6 - 9	+0.4432	+0.4432	0.5	1.0239	0.5119
14 - 12	+0.4432	-0.4432	1.0	1.0004	1.0004
5 - 3	-0.4432	+0.4432	1.0	1.0117	1.0117
16 - 10	-0.4432	+0.4432	1.0	0.9968	0.9968
2 - 8	+0.4432	-0.4432	1.0	0.9806	0.9806
13 - 16	0	0	1.5	0.9879	1.4819
1 - 4	0	0	1.5	1.0032	1.5048
1 - 8	+0.4432	-0.4432	1.5	0.9955	1.4925

By examining the Laue orientation of the crystal, one derives the transformation.

$$\Delta x_o = .77544\,\Delta x_o' + .62206\,\Delta y_o' + .10830\,\Delta z'$$

$$\Delta y_o = -.45936\,\Delta x_o' + .43809\,\Delta y_o' + .77270\,\Delta z'$$

$$\Delta z_o = .43322\,\Delta x_o' - .64894\,\Delta y_o + .62546\,\Delta z'$$

Transforming, we have:

Leads	Δx_o cm	Δy_o cm	Δz_o cm
6 - 9	.6748	.3861	.2246
14 - 12	.1763	.3752	1.1053
5 - 3	.0416	1.1795	.1532
16 - 10	.0400	1.1680	.1439
2 - 8	.1742	.3599	1.0929
13 - 16	.1605	1.1451	.9269
1 - 4	.1630	1.1628	.9412
1 - 8	.2296	.7555	1.4131

Also from the Laue picture, we have:

$\cos \phi_o = \cos (\angle xz') = .10830$ $\quad\quad$ $\cos \lambda_o = \cos (\angle yz') = .77270$

$\sin \chi_o = \cos (\angle zz') = .62546$ $\quad\quad$ $\sin \lambda_o = .63475$

$A_o = .6171 \text{ cm}^2$ $\quad\quad$ $\cos \lambda_o / \sin \chi_o = 1.23541$

Electrical data for the grown specimen follows (resistance) represents two or more readings; spread of readings is indicated.

Leads	300°K R($\mu\Omega$)	4°K R($\mu\Omega$ x 10^2)
6 - 9	2.0384 ± .0003	0.6479 ± .0013
14 - 12	3.9835 ± .0001	1.2564 ± .0021
5 - 3	4.0284 ± .0000	1.2661 ± .0003
16 - 10	3.9690 ± .0014	1.2937 ± .0023
2 - 8	3.9045 ± .0005	1.2398 ± .0002
13 - 16	5.9006 ± .0002	1.8687 ± .0112
1 - 4	5.9918 ± .0001	1.9229 ± .0072
1 - 8	5.9458 ± .0001	1.8664 ± .0207

Using the readings at 4°K, one gets the following simultaneous equations from $\cos(\angle xz')\rho_x \Delta x + \cos(\angle yz')\rho_y \Delta y + \cos(\angle zz')\rho_z \Delta z = RA$

Leads	$\cos(\angle xz')\Delta x$		$\cos(\angle yz')\Delta y$		$\cos(\angle zz')\Delta z$		R
6 - 9	.0731	$\frac{\rho_x}{A}$ +	.2983	$\frac{\rho_y}{A}$ +	.1405	$\frac{\rho_z}{A}$ =	.0648
14 - 12	.0191		.2899		.6913		.1256
5 - 3	.0045		.9114		.0958		.1266
16 - 10	.0043		.0025		.0900		.1294
2 - 8	.0189		.2781		.6836		.1240
13 - 16	.0174		.8848		.5797		.1869
1 - 4	.0177		.8985		.5887		.1923
1 - 8	.0249		.5838		.8838		.1866
	cm		cm		cm		$\mu\Omega$ x 10

Using a least square method of solution, one gets

$\rho_x = .1257A = 7.76 \times 10^{-9}\ \Omega$ cm

$\rho_y = .1281A = 7.91 \times 10^{-9}\ \Omega$ cm

$\rho_z = .1244A = 7.68 \times 10^{-9}\ \Omega$ cm

Check these values with the experimental values:

Leads	R(calculated)($\mu\Omega$ x10)	R(experimental)($\mu\Omega$ x10)
6 - 9	.0649	.0648
14 - 12	.1255	.1256
5 - 3	.1293	.1266
16 - 10	.1273	.1294
2 - 8	.1230	.1240
13 - 16	.1876	.1869
1 - 4	.1905	.1923
1 - 8	.1878	.1866

The specimen was now given a 16 o/o extension. To calculate the new resistivities, we proceed as follows:

$\epsilon = 1.159$ $\qquad A_\epsilon = A_o/\epsilon = .5324$

$\cos \phi_\epsilon = \cos \phi_0 / \epsilon = .09344$ $\quad \sin \lambda_\epsilon = \dfrac{\sin \lambda_0}{\epsilon} = .54767$

$\sin \chi_\epsilon = \dfrac{\sin \chi_0}{\epsilon} = .53965$ $\quad \cos \lambda_\epsilon = .83669$

$\cos \lambda_\epsilon / \sin \chi_\epsilon = 1.55043$ $\quad a_\epsilon = \dfrac{\cos \lambda_\epsilon}{\sin \chi_\epsilon} - \dfrac{\cos \lambda_0}{\sin \chi_0} = .31502$

$\Delta x_\epsilon = \Delta x_0 \qquad \Delta y = \Delta y_0 + a_\epsilon \Delta z_0 \qquad \Delta z_\epsilon = \Delta z_0$

Leads	Δy_0	a_ϵ	Δz_0		R($\mu\Omega$ x 10^2) at 4°K
6 - 9	.3861		.2246	-.4569	1.378
14 - 12	.3752		1.1053	.7234	3.079
5 - 3	1.1795		.1532	1.2278	2.848
16 - 10	1.1680	+ .31502	.1439	1.2133	2.751
2 - 8	.3599		1.0929	.7042	2.927
13 - 16	1.1451		.9269	1.4371	4.298
1 - 4	1.1628		.9412	1.4593	4.365
1 - 8	.7555		1.4131	1.2007	4.423

$\Delta y_\epsilon =$

This gives the simultaneous equation:

Leads

6-9	.0631		.3823		.1212		.1378
14-12	.0165		.6053		.5965		.3079
5-3	.0039		1.0273		.0827		.2848
16-10	.0037		1.0152		.0777		.2751
2 - 8	.0163	$\dfrac{\rho_x}{A}$ +	.5892	$\dfrac{\rho_y}{A}$ +	.5898	$\dfrac{\rho_z}{A}$ =	.2927
13-16	.0150		1.2024		.5002		.4298
1-4	.0152		1.2210		.5079		.4365
1-8	.0215		1.0046		.7626		.4423

These are solved as previously.

APPENDIX II

It is interesting to compare the relative resistivity contributions of dislocations and vacancies. Using the values quoted in the introductory remarks, we take the resistivity increase due to dislocations to be $\Delta\rho_d = 0.4\times10^{-14}N\ \mu\Omega\text{cm}$, where N is the number of dislocations per cm^2, and $\Delta\rho = 1.3\ \mu\Omega\text{cm}$ per percent of vacancies. In one cm^3 there are approximately 0.8×10^{23} atoms. Thus 1 percent of vacancies is equivalent to 0.8×10^{21} vacancies per cm^3. Along a row of atoms there are $1/a = 1/2.5\times10^{-8} = 4\times10^{7}$ atoms. Thus 1 percent of vacancies is equivalent to $0.8\times10^{21}/4\times10^{7} = 2\times10^{13}$ lines of vacancies per cm^3. Now 2×10^{13} dislocation lines in 1 cm^3 would give a resistivity increase of $0.4\times10^{-14} \times 2\times10^{13} = 0.8\times10^{-1}\ \mu\Omega\text{cm}$; therefore the ratio of increases for one percent of vacancies compared to an equivalent density of dislocations if $1.3 / 0.08 = 15.7$

Thus we deduce that vacancies are on the order of fifteen times more effective than dislocations in producing resistivity increases.

APPENDIX III

The present investigation suggests several possible new experiments:

1. A complete study of the dependence of resistivity increase on stress in face-centered cubic and hexagonal metals should yield information concerning the interaction of dislocations on different glide planes. This has already been discussed.

2. The stress-strain behavior in aluminum should be pursued further at low temperatures. This should be combined with annealing studies.

3. Parker and Washburn[48] have deformed zinc in pure shear. To further reduce the complication of latent slip systems, it may be desirable to look for anisotropic changes in resistivity, straining in a similar manner.

4. Salkovitz and Koehler[49] have examined asterism of Laue spots after kinking zinc. For an xray beam perpendicular to the bend axis, the spots are smeared radially; for a beam parallel to the bend axis, the spots are smeared tangentially. This is in line with the belief that an array of positive (or negative) edge dislocations from a kink corner. P. Haasen[50] suggests that slip proceeds simultaneously on all slip planes in aluminum, even at lowest stresses. This could account for resistivity isotropy without ruling out dislocations as a major source of resistivity increase. By examining asterism in aluminum relative to different directions in the lattice (i.e., relative to different slip planes), this matter could be further clarified.

5. It has been suggested here that crossing screw dislocations may form the major source of vacancy production. Another source may

be jogs in dislocations. To study the creation of vacancies, it would be useful to be able to introduce an excess of one type of dislocation into the lattice. An experiment suggested by Koehler is to compare the resistivity behavior of specimens that have been previously twisted to introduce screw dislocations and specimens that have been bent to introduce edge dislocations.

6. Vacancies surely affect hardness. Since quenching from high temperatures presumably yields a high concentration of vacancies it would be interesting to quench to temperatures just above and below the place where these vacancies become mobile and examine the stress-strain behavior in these regions.

7. The aging phenomena should be further examined.

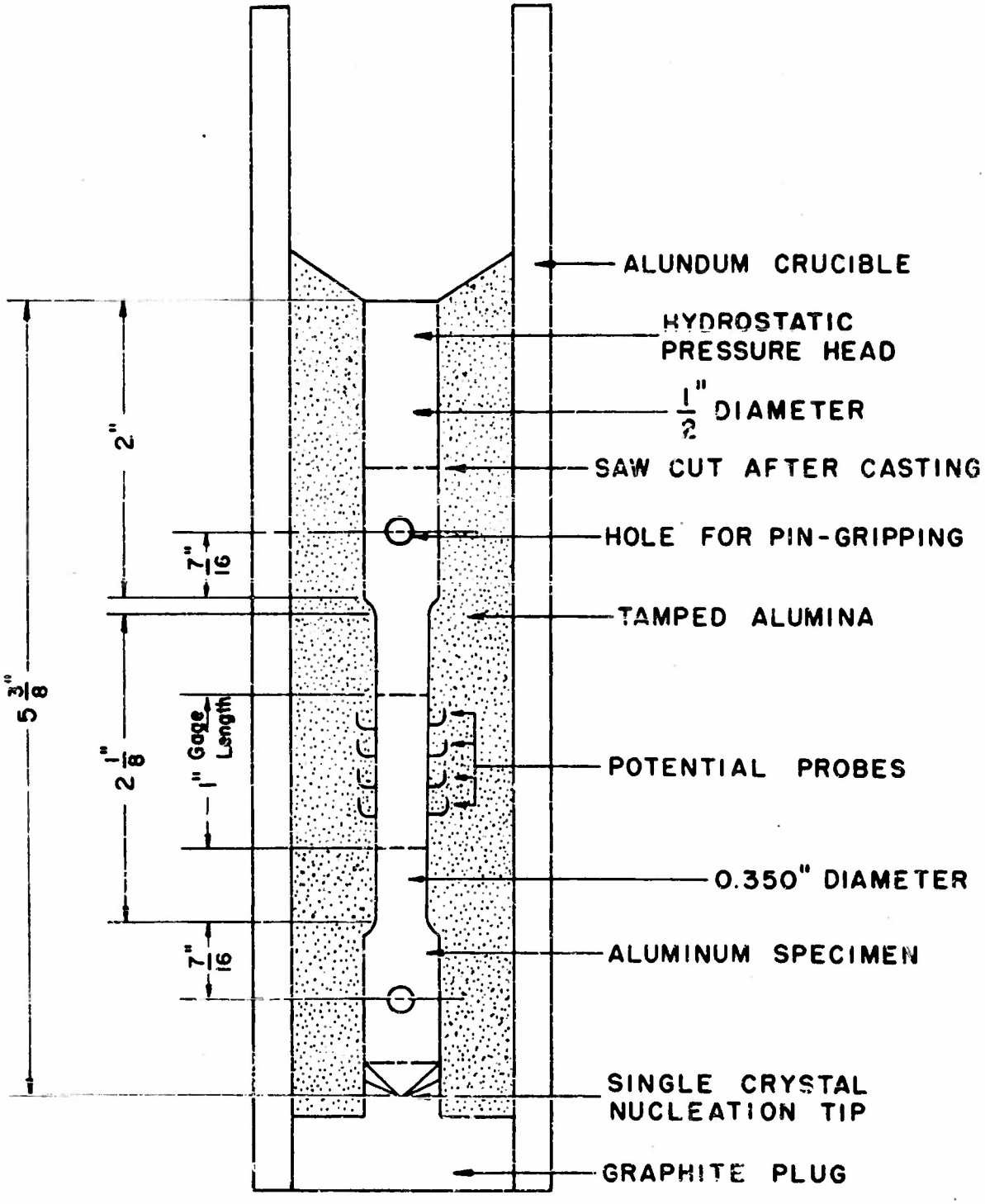

FIGURE 1

Section through specimen inserted in crucible for casting.

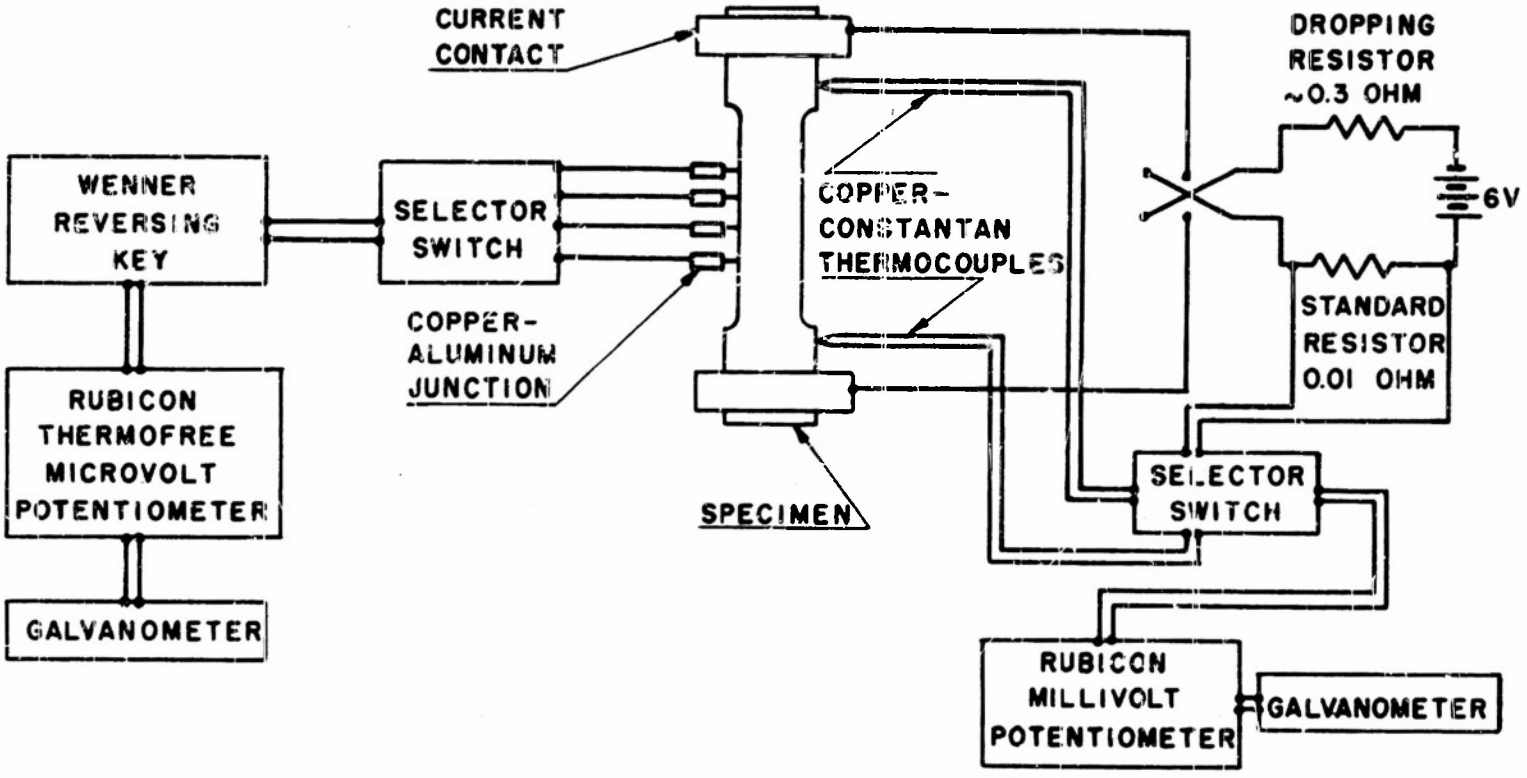

FIGURE 2

Schematic of resistance measurement circuit.

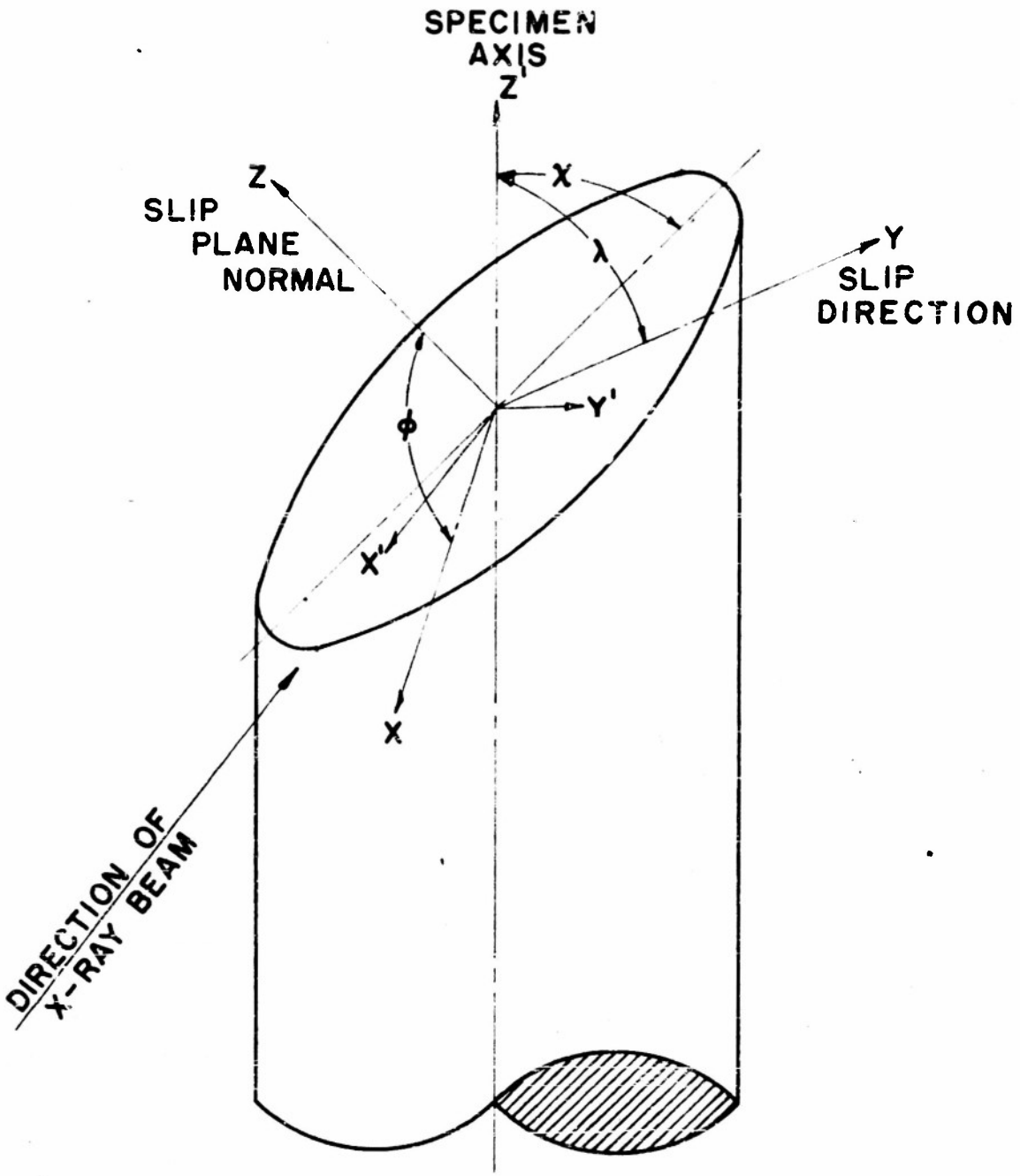
SPECIMEN
AXIS
Z'
Z
SLIP
PLANE
NORMAL
X
λ
Y
SLIP
DIRECTION
Y'
φ
X'
X
DIRECTION OF
X-RAY BEAM

FIGURE 3

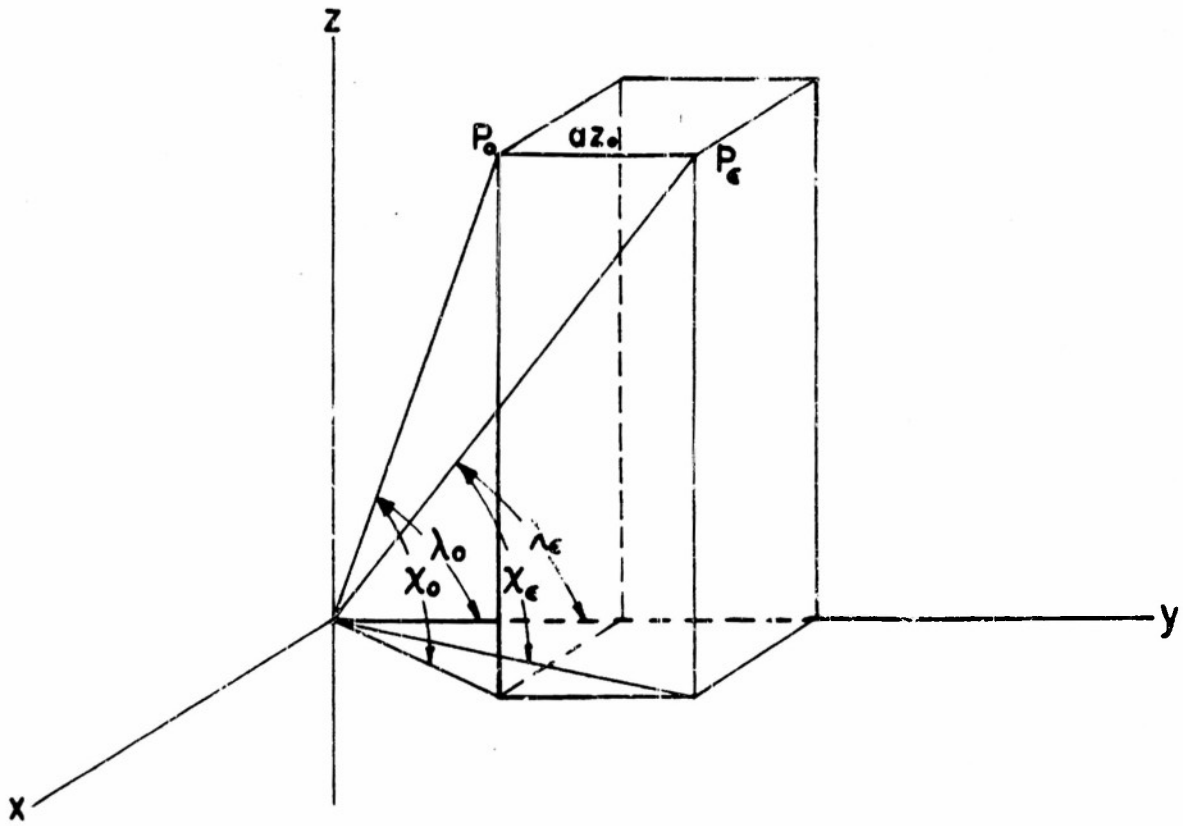

FIGURE 4

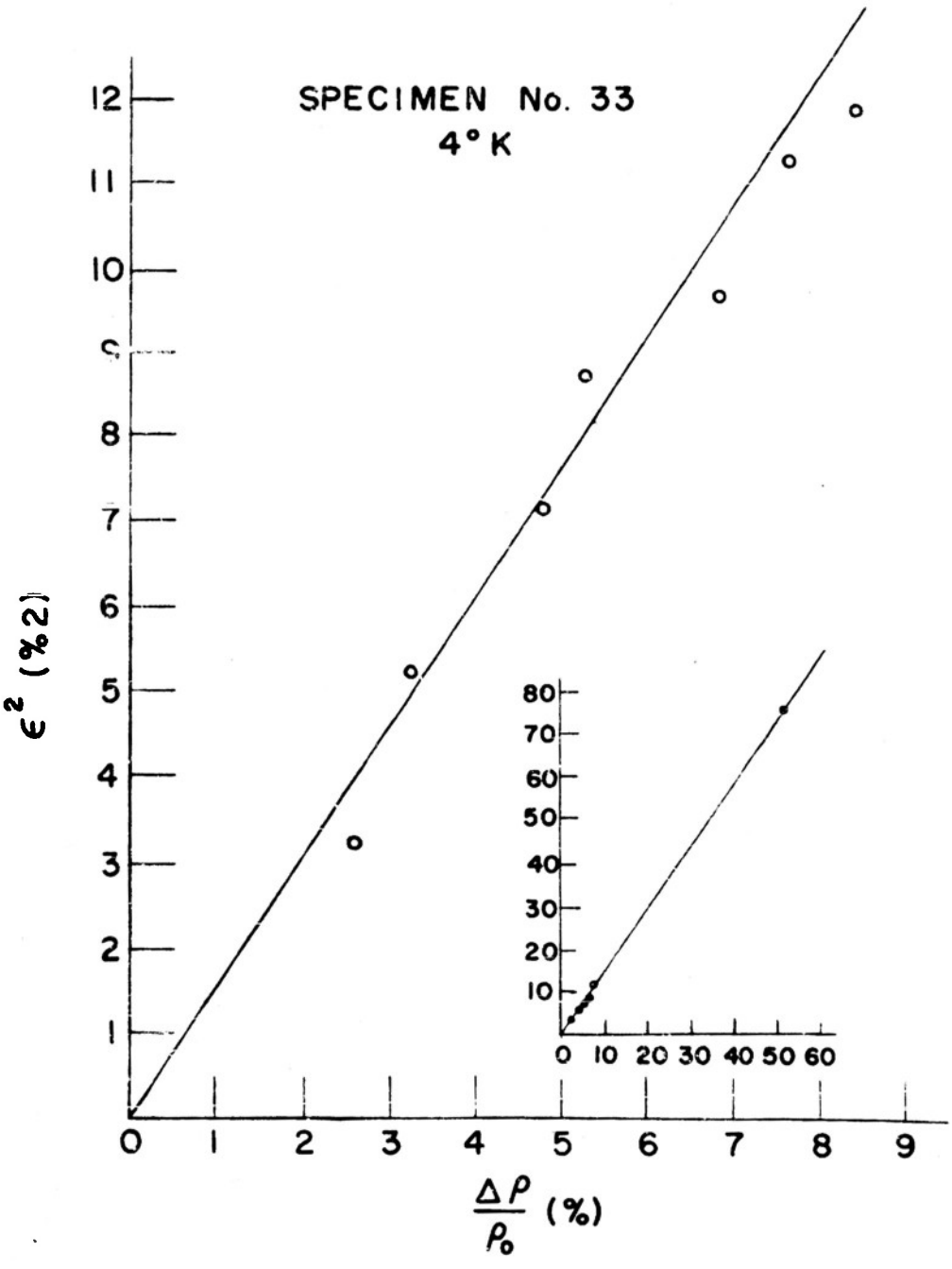
SPECIMEN No. 33
4° K
ϵ^2 (%2)
12
11
10
9
8
7
6
5
4
3
2
1
0 1 2 3 4 5 6 7 8 9
$\frac{\Delta \rho}{\rho_0}$ (%)
80
70
60
50
40
30
20
10
0 10 20 30 40 50 60

FIGURE 5

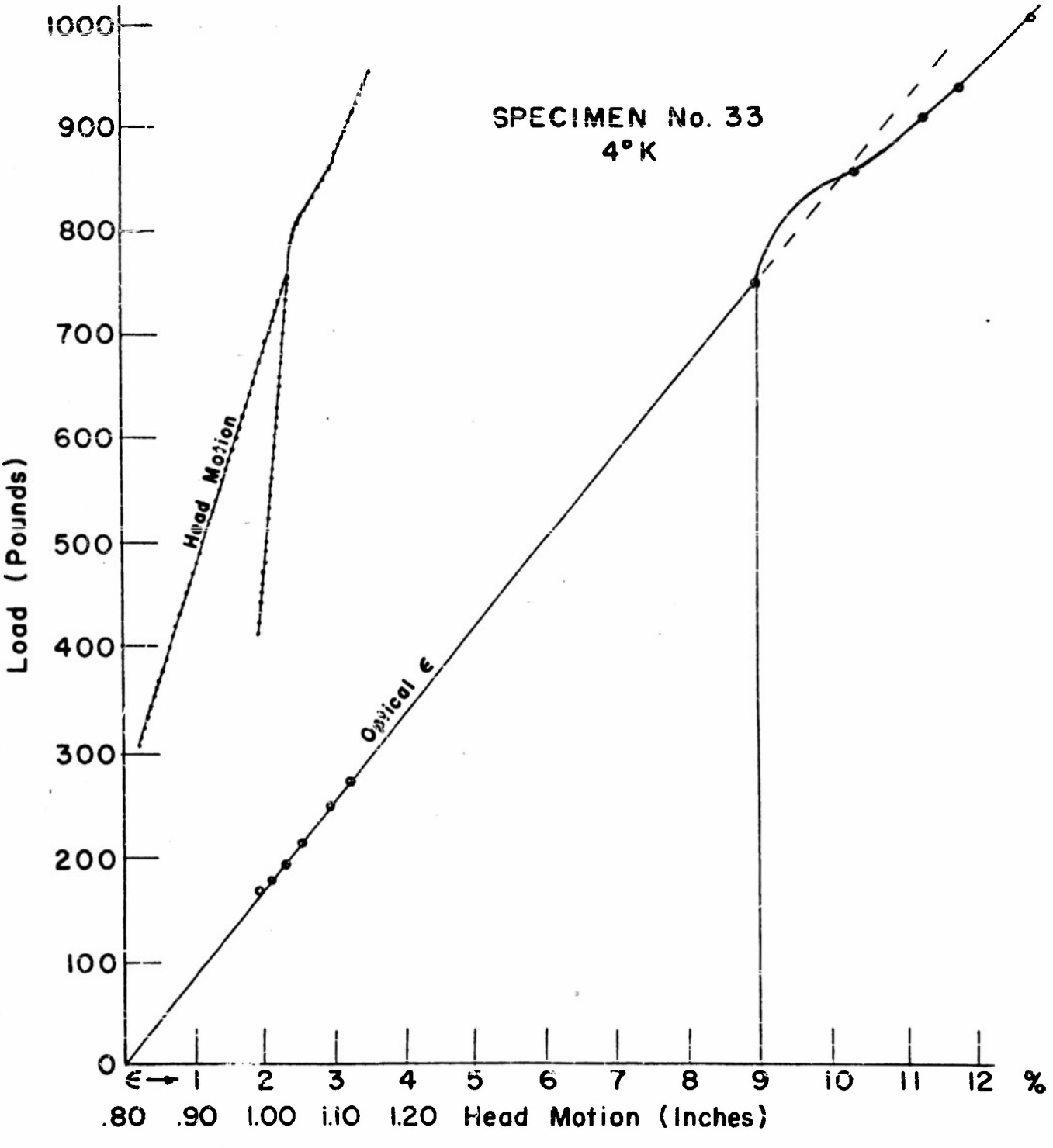
SPECIMEN No. 33
4°K
Load (Pounds)
1000
900
800
700
600
500
400
300
200
100
0
Head Motion
Optical ε
ε → 1 2 3 4 5 6 7 8 9 10 11 12 %
.80 .90 1.00 1.10 1.20 Head Motion (Inches)

FIGURE 6

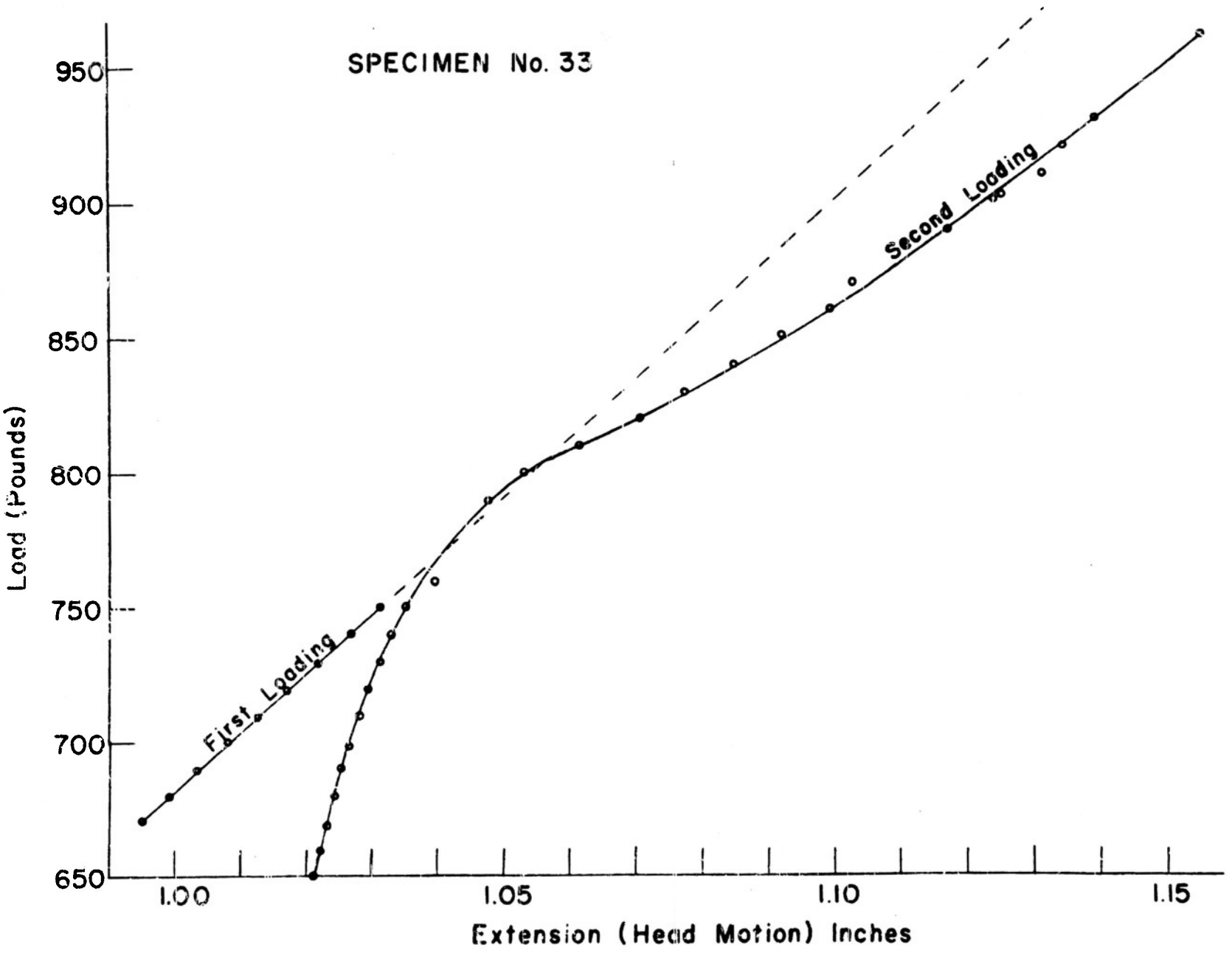
SPECIMEN No. 33
950
900
850
800
750
700
650
Load (Pounds)
First Loading
Second Loading
1.00
1.05
1.10
1.15
Extension (Head Motion) Inches

FIGURE 7

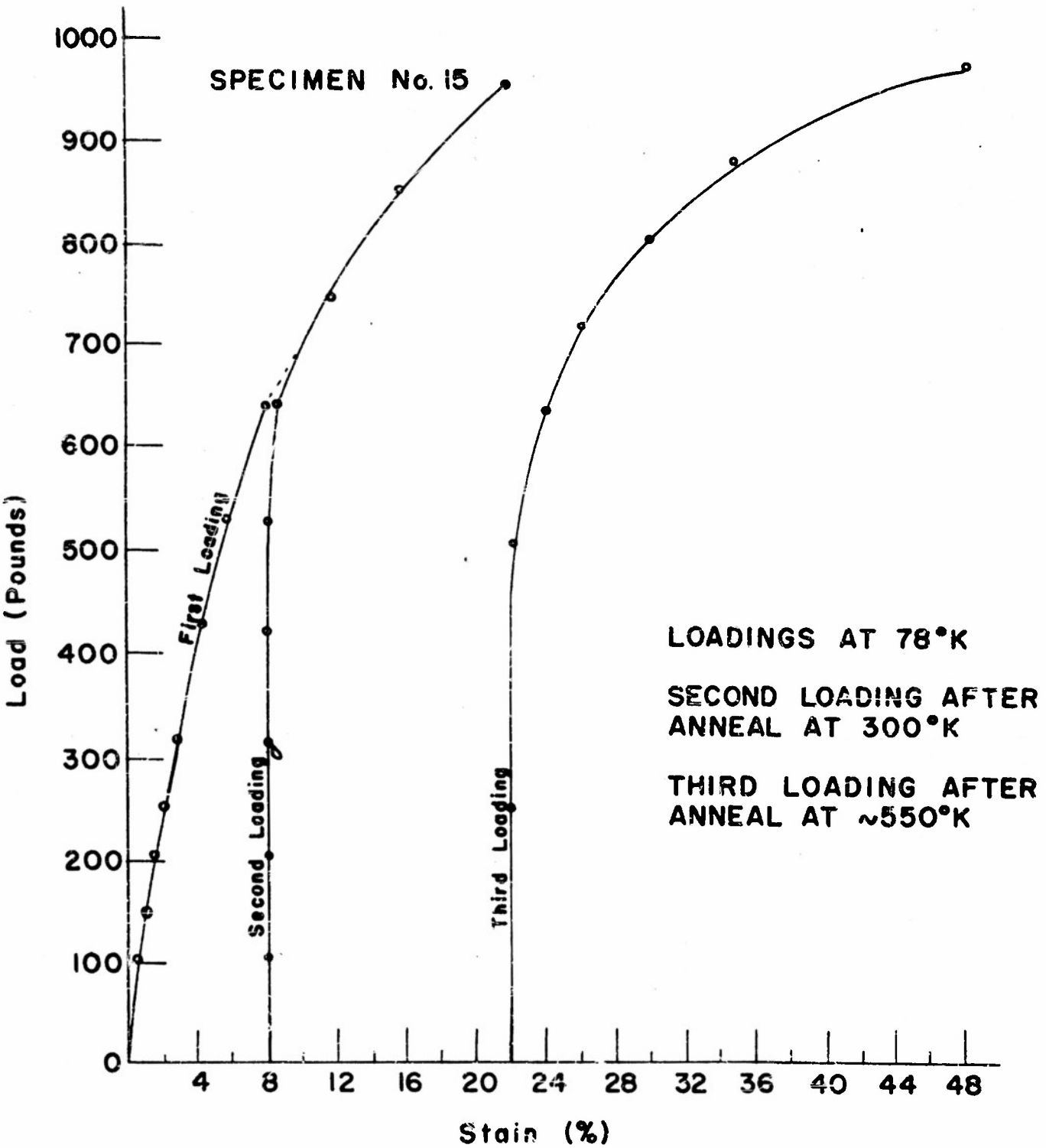
SPECIMEN No. 15
Load (Pounds)
1000
900
800
700
600
500
400
300
200
100
0
First Loading
Second Loading
Third Loading
4
8
12
16
20
24
28
32
36
40
44
48
Stain (%)
LOADINGS AT 78°K
SECOND LOADING AFTER ANNEAL AT 300°K
THIRD LOADING AFTER ANNEAL AT ~550°K

FIGURE 8

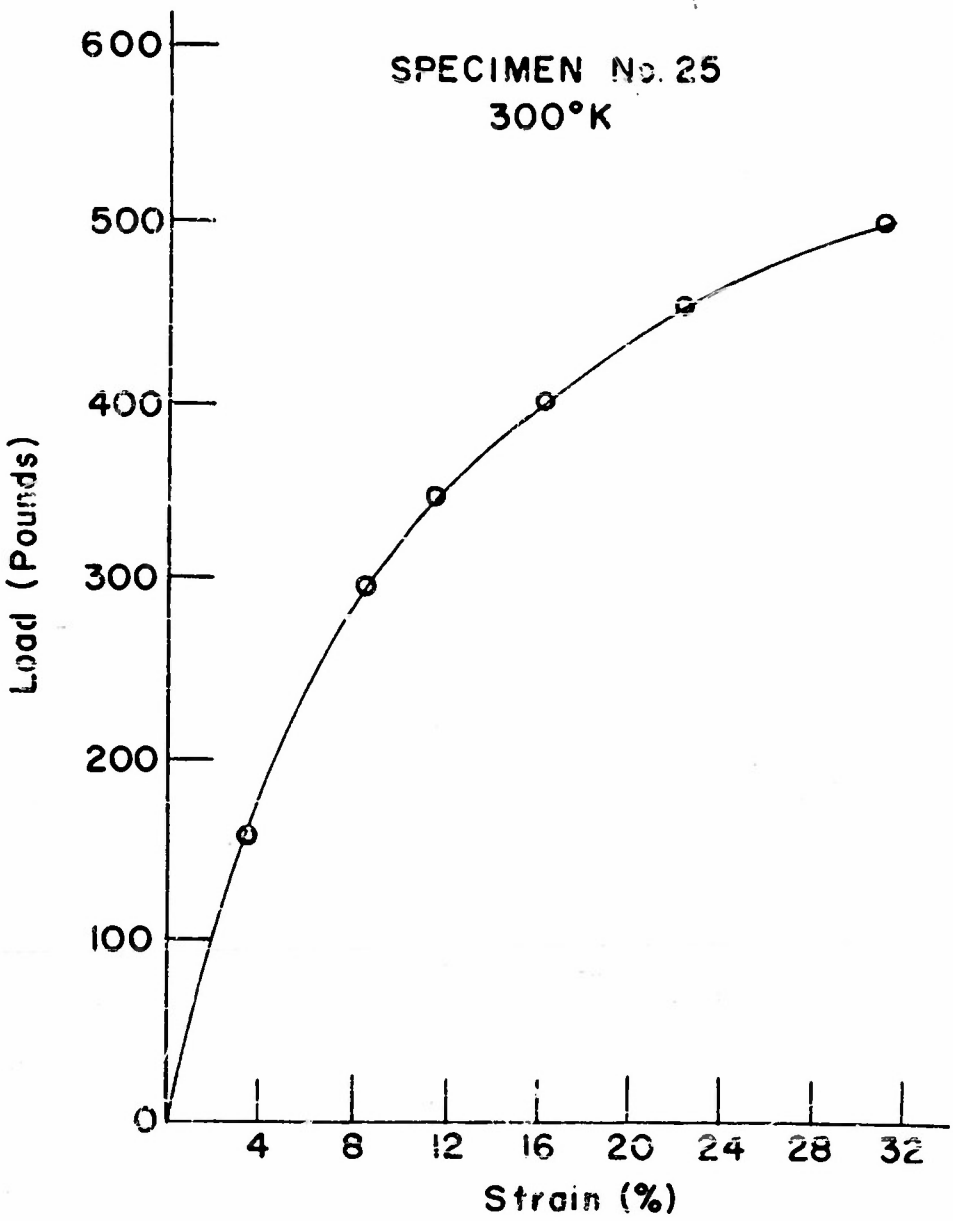
SPECIMEN No. 25
300°K
600
500
400
300
200
100
0
Load (Pounds)
4
8
12
16
20
24
28
32
Strain (%)

FIGURE 9

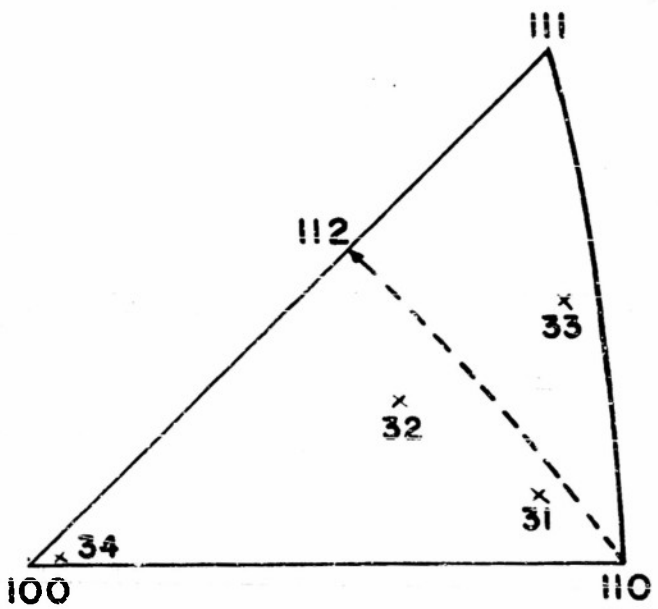

FIGURE
Specimen Orientation